

Motivation and Initial Results from SPINOR in the Near Infrared

Hector Socas-Navarro, David Elmore & Bruce W. Lites *
High Altitude Observatory, NCAR †

October 1, 2004

Abstract. SPINOR is a new spectro-polarimeter that will serve as a facility instrument for the Dunn Solar Telescope at the National Solar Observatory. This instrument is capable of achromatic operation over a very broad range of wavelengths, from ~ 400 up to 1600 nm, allowing for the simultaneous observation of several visible and infrared spectral regions with full Stokes polarimetry. Another key feature of the design is its flexibility to observe virtually any combination of spectral lines, limited only by practical considerations (e.g., the number of detectors available, space on the optical bench, etc). SPINOR is scheduled for commissioning by the end of 2005. In this paper we report on the current status of the project and present actual observations of active regions in the Ca II infrared triplet and the He I multiplet at 1083 nm.

Keywords: instrumentation: polarimeters, polarization, telescopes, Sun: magnetic fields, Sun: photosphere, Sun: chromosphere

1. Introduction

The new breed of spectro-polarimeters scheduled to begin operation in the next few years make the present a very exciting time for solar physics. Examples of these instruments are SOLIS (Keller 1998), Solar-B (Lites et al. 2001), POLIS (Schmidt et al. 2003), Sunrise (Solanki et al. 2003), and the DLSP (Sankarasubramanian et al. 2003). All these instruments, however, are highly specialized and operate under fixed conditions, either with the aim of performing synoptic observations or to optimize for spatial resolution. While these aspects are very important for the future advance of solar physics, we feel that there is also a need for an “experiment-oriented” type of instrument. By this we mean an instrument that provides enough flexibility to implement more or less arbitrary optical arrangements at the observer’s request. Such an instrument should allow researches to observe any given spectral line (or combinations of lines), either at the disk or off the limb at a

* Visiting Astronomers, National Solar Observatory, operated by the Association of Universities for Research in Astronomy, Inc. (AURA), under cooperative agreement with the National Science Foundation.

† The National Center for Atmospheric Research (NCAR) is sponsored by the National Science Foundation



diverse range of wavelengths. One should be able to modify parameters like spatial resolution, spectral dispersion, integration times, etc, in order to address a broad range of scientific problems. In some sense, operating an instrument of this kind is like setting up an experiment in a laboratory. Optical components and detector systems are arranged on an optical bench to investigate some specific problem.

For more than a decade, the highly successful Advanced Stokes Polarimeter (ASP, Elmore et al. 1992) has provided these capabilities at *visible* wavelengths. The Spectro-Polarimeter for Infrared and Optical Regions (SPINOR) will replace the ASP as the experiment-oriented spectro-polarimeter on the Dunn Solar Telescope (DST) at the National Solar Observatory (NSO), Sunspot, NM, USA. SPINOR is currently under development by the High Altitude Observatory and the National Solar Observatory. It has been conceived with flexibility as a top priority and intends to fill this gap in the next-generation solar instrumentation. The new instrument will replace and enhance the capabilities of the ASP.

Table I below provides some specifications for SPINOR. The most important enhancement over the ASP is the ability to observe simultaneously in the visible *and* the near infrared. Higher spatial resolution than was available over most of the life of the ASP is now possible thanks to the high-order adaptive optics (AO) system (Rimmele 2000) developed for the DST. Two different detectors will be available at commissioning time (scheduled for the end of 2005): a PixelVision Pluto 652x488 thinned back illuminated split frame transfer CCD, 60 frames per second readout rate (hereafter Pluto) and a Sarnoff CAM1M100, 1024x512, thinned back illuminated split frame transfer CCD, 100 frames per second readout rate. These will be fully dedicated for observations between 400 and ~ 900 nm. The SPINOR optics allows for an even broader range of wavelengths, up to $1.6 \mu\text{m}$. We plan to take advantage of this in future observations by using an HAO Rockwell infrared camera that is shared with other HAO projects. The modular design of the instrument control will allow for additional detectors to be attached to SPINOR using NSO's Virtual Camera interface.

The present configuration of the instrument, used in the engineering run reported here, does not include the Sarnoff or the Rockwell cameras. For this run we used the ASP control computers and detectors alongside the Pluto camera. With this configuration we were able to demonstrate SPINOR's achromatic spectro-polarimetry up to 1083 nm.

This paper is organized as follows. Section 2 discusses the scientific motivations for the development of SPINOR. Section 3 presents a description of the polarimeter with some details on the new achromatic optics. The polarimetric calibration of the system consisting of the tele-

scope and the polarimeter is explained in section 3.2. Some observations taken during an engineering run in June 2004 are presented in section 4. Finally, section 5 presents the main conclusions of our work and some future perspectives.

2. Scientific Rationale

The main scientific driver behind the development of SPINOR is to expand the present ASP magnetometric capabilities into the higher solar atmosphere (chromosphere and corona). However, its infrared coverage is also of great relevance for the study of problems associated with photospheric magnetism. Below we summarize some of the major scientific problems for which SPINOR is particularly suited, which cannot be pursued using the ASP (or other existing instruments). However, being that this an experiment-oriented instrument designed for maximum versatility, its most important applications might be some that we cannot envision at this time

2.1. PHOTOSPHERIC MAGNETISM

Recent investigations of photospheric fields in the infrared often reveal a different picture from conventional visible observations. A remarkable example is the finding of supersonic flows in the penumbrae of sunspots by del Toro Iniesta et al. (2001) in data from the Tenerife Infrared Polarimeter (TIP). Such strong flows had never been observed in the visible, with the exception of the peculiar δ -configuration sunspots (Martínez Pillet et al. 1994), and flows near pores (Lites et al. 2001).

Perhaps the most puzzling observations of photospheric fields in the infrared are those of the quiet sun, particularly outside the magnetic network (the region sometimes referred to as the photospheric inter-network). Visible observations indicate that most of the fields in this region are strong (~ 1.3 kG), but concentrated into very small areas ($\sim 1\%$ of the pixel; see Socas-Navarro and Sánchez Almeida 2002 and references therein). However, recent infrared observations (Lin 1995; Lin and Rimmele 1999; Khomenko et al. 2003) suggest that most of the fields are weak (~ 400 G) and diffuse. These contradictory results have sparked a controversy on the true nature of quiet sun fields. This issue is an important one, since our current understanding indicates that most of the solar magnetic flux (even at solar maximum) is located in the quiet sun outside of active regions, and it is likely that the evolution of this flux plays a role in the heating of the upper atmosphere. A possible solution to the observational contradiction has been proposed by Socas-Navarro (2003) and Socas-Navarro and Sánchez Almeida (2003). It

turns out that the observations may be explained easily by a small-scale distribution of fields, beyond the spatial resolution of the observations, having intermixed weak and strong fields. Moreover, these authors showed that the actual sub-pixel distribution of the field can be inferred from simultaneous visible and infrared observations (like those from SPINOR).

The results of Socas-Navarro and Sánchez Almeida (2003) may be extrapolated to other physical scenarios in which different field strengths coexist within the resolution element of the observations. Another example where this strategy would be very useful is the investigation of sunspot penumbrae. It is presently believed (see, e.g., Schlichenmaier 2002; Sánchez Almeida and Bonet 1998) that a penumbra is formed by a large number of thin radial filaments embedded in a magnetic environment, with the filaments having weaker and more horizontal fields and channeling the cool siphon flows traditionally observed as the Evershed effect. The actual size, properties and origin of these filaments are still a subject of intense debate (Martínez Pillet 2000; Sánchez Almeida 2001; Martínez Pillet 2001), but it seems well established that they are not spatially resolved in the observations. The ability to infer spatially-unresolved distributions of the magnetic field from simultaneous visible and infrared observations would provide important clues on the structure of the penumbra.

Innovative new diagnostics of solar magnetic fields are emerging as a result of parallel theoretical and observational advances. In a recent effort to understand the anomalous polarization signals observed in some spectral lines, López Ariste et al. (2002) studied the hyperfine structure induced in the atomic energy levels by the nuclear spin, and its effects on the polarization transfer process. They demonstrated that the signature imprinted by the hyperfine structure on some spectral lines has an important potential for magnetic field diagnostics. Some of the most interesting lines lay in the wavelength domain between 800 and 1500 nm. Examples are the Rb I D1 line at 794 nm, which shows a combination of hyperfine structure and isotopic mix, or the Mn I lines at 870 nm, and in the infrared at 1.29, 1.33 and 1.52 μm .

2.2. CHROMOSPHERIC AND CORONAL MAGNETISM

A new global picture of solar magnetism is emerging from the seemingly disparate observational domains of photospheric small-scale magnetic fields and the diffuse, voluminous magnetic structure of the solar corona. The observation and interpretation techniques used for photospheric and coronal studies are markedly different. To further the development of this global view, we identify a key missing ingredient:

an in-depth investigation of the interface layer, the chromosphere. Observational capability for chromospheric vector magnetic fields and the associated dynamics has been lacking because most interesting and/or useful lines lie outside the wavelength coverage range of most solar polarimeters (it should be noted, however, that successful investigations of prominence fields have been carried out recently; e.g. Casini and López Ariste 2003). Observable lines either form too low in the chromosphere (e.g., the Mg I *b*-lines) or their polarization transfer is still not well understood (e.g., H_α).

SPINOR would open new perspectives for chromospheric investigations with its ability to observe the full polarization state of the Ca II infrared triplet, around 854 nm. These lines are the best candidates for chromospheric diagnostics, at least in the Zeeman regime, due to their relatively simple formation physics, their long wavelengths (which results in stronger Zeeman signals), and the valuable information they carry on the thermal and magnetic conditions of the higher atmosphere (Uitenbroek 1989; Socas-Navarro et al. 2000c; Socas-Navarro et al. 2000b). They are also sensitive to the Hanle effect, which provides complementary diagnostics on the weaker (~ 1 G) fields, and have been successfully modeled by Manso Sainz and Trujillo Bueno (2001).

Finally, the He I multiplet at 1083 nm is of great interest for chromospheric and coronal studies. This line is seen in emission in prominences and in absorption in filaments, with strong polarization signals arising from both Hanle and Zeeman effect. SPINOR would be able to provide full spectro-polarimetry at 1083 nm, which implies the potential to investigate the magnetic and dynamic conditions of these structures. Other interesting coronal lines that may be accessible for observations are the two Fe XIII lines at 1074 nm, although these may not be visible using a traditional solar telescope.

3. Description of the instrument

SPINOR is based on the design of the ASP, which uses a rotating waveplate as a modulator and a polarization beam splitter as a dual-beam analyzer. All of the polarization optical components, however, have been replaced by new achromatic ones. SPINOR utilizes the ASP calibration/modulation unit (cal/mod) at the exit port of the DST, high-order AO, and the Horizontal Spectrograph.

Since SPINOR operates over a much wider wavelength range compared to ASP, it was deemed necessary to allow SPINOR to use a selection of gratings. Depending upon the desired spectral line and spectral resolution, different gratings may be selected. Higher blaze

Table I. Performance comparison between SPINOR and ASP

Parameter	ASP	SPINOR
Calibratable wavelength range (nm)	450-750	400-1600
Field of view along slit (arc seconds)	80	120
Quantum efficiency	400 nm	0.01
	700 nm	0.32
	1080 nm	0.00
	1600 nm	0.00
		0.03, 0.60*
		0.60*
		*(with suitable IR camera)
Read noise (electrons)	50	25

angle gives higher spectral resolution for the same spatial sample size. Since SPINOR will operate with AO, its design favors a higher spatial resolution than the ASP. Since it is a general-purpose research instrument, it cannot be optimized for a single line, so the SPINOR spatial resolution is not as high as that attainable by the new DLSP. These spectrograph issues lead typically to a spectrograph using a $40\ \mu\text{m}$ slit and 1000 mm camera lens. The observations reported in this paper were carried out using the 308.57 lines/mm grating with a blaze angle of 52° .

3.1. SPECIFICATIONS

SPINOR has been conceived keeping versatility as the highest priority in order to allow for a broad range of potential applications. The project is being developed in a way that allows the ASP to remain operational until the new instrument is completed. Its most important features are:

- Achromatic optics from 400 to 1600 nm offer the capability of simultaneous observations at diverse wavelengths. This extended range represents an important improvement over that of the ASP. Its potential scientific benefits have been discussed in more detail in section 2.
- Detectors with higher quantum efficiency and lower noise than those in ASP allowing for higher signal to noise observations.
- Use of state-of-the-art components, electronic systems, computers, detectors and software. Deployed over 12 years ago, ASP's technology is now 15 or more years old, and some of its systems are starting to fail. Both routine maintenance tasks and normal

operation are compromised because many replacement parts are no longer available. The SPINOR system will be more stable and suffer significantly less downtime. Data products will also be easier to handle (e.g., using DVDs instead of magnetic tapes, simpler analysis procedures, etc), an improvement that will greatly facilitate the science and make the instrument more accessible to a broader user community.

- Open and modular optical design, with room on the optical bench to incorporate and/or replace components. SPINOR will be deployed at the DST as a set of instrument modules with “virtual” cameras, a concept that NSO has developed for the DLSP and other DST instrumentation. This will allow diverse and complex observations, combining SPINOR with other DST instruments. The control software will be fully customizable for a broad variety of observing modes (although several pre-defined modes will exist for frequently used configurations).

3.2. CALIBRATION

The calibration procedure for SPINOR consists in the determination of the Mueller matrices of the telescope (\mathbf{T}) and the polarimeter (\mathbf{X}). Any solar Stokes vector \mathbf{s}_{in} is observed as \mathbf{s}_{out} :

$$\mathbf{s}_{\text{out}} = \mathbf{X}\mathbf{T}\mathbf{s}_{\text{in}}. \quad (1)$$

The Mueller matrix of the polarimeter depends on the particular instrumental configuration and varies significantly in between observing runs (sometimes even from one day to the next). For this reason, polarimeter calibration operations are done typically once a day, or even more often if changes are made to the instrument. Fortunately, calibration operations do not take too long (~ 20 minutes). A calibration linear polarizer and retarder are mounted following the telescope exit window. These are used to polarize the light beam in various known states. The known input vectors and the observed outputs are used in a least-squares fitting procedure to determine the matrix elements of \mathbf{X} . This is essentially the same procedure that was used for the ASP calibration, which is explained in the paper by Skumanich et al. (1997) and will not be repeated here. The only difference is that the calibration polarizer and retarder are now almost entirely achromatic over the broad wavelength range of SPINOR. The retardance of the calibration retarder and the orientation of its fast axis are taken as free parameters of the fit, in order to account for wavelength variations and possible mounting inaccuracies.

The telescope calibration requires an entire day of observations at different positions of the Sun on the sky. This needs to be done at least every time the turret mirrors are recoated, and desirably every few months. We have devised a new method that departs significantly from that of Skumanich et al. (1997). The telescope is modeled as a function of 9 free parameters: the entrance window retardance and axis orientation; the turret mirrors retardance and ratio of reflectivities (rs/rp); the main mirror retardance and rs/rp ; the exit window retardance and axis orientation; and finally the relative rotation between the telescope and the polarimeter (see Skumanich et al. 1997 for an explanation of these parameters).

An array of achromatic linear polarizers, placed in front of the entrance window, is used to introduce known states of polarization in the system. These vectors are measured at various times of the day, covering a wide range of the three variable angles of the telescope: turret azimuth, elevation and table rotation. Again, a least-squares fit is used to determine the free parameters of the model.

The new SPINOR technique uses a cross-dispersing prism placed before one of the detectors to record the various overlapping orders simultaneously (shown in Fig 1). In this manner we are able to obtain telescope calibration data for many wavelengths at once. Instead of fitting each set of parameters independently for each wavelength, we take a fully-consistent approach whereby the entire dataset is fit using a wavelength-dependent model. Some parameters (window retardances and mirror properties) are allowed to vary with wavelength in the fit, up to the third order in λ . The rest of the parameters are wavelength-independent. This model has sufficient freedom to reproduce the measured vectors in the entire dataset and at the same time provides a consistent model of the telescope. Table II shows the various telescope parameters obtained from our calibration at three different wavelengths.

4. Observations

The observations presented in this paper were obtained during an engineering run on June 2004 with the following setup. The ASP cameras were configured to record the Ca II lines at 849.8 and 854.2 nm (plus some other photospheric and telluric lines blended in the wings of the Ca lines). The new Pluto camera was observing at 1083.0 nm, including the He I multiplet, two photospheric lines and a telluric line. We aligned the camera chips so that the broad Ca lines would fall near the edge of the chip. In this manner we can record some wing “continuum” on

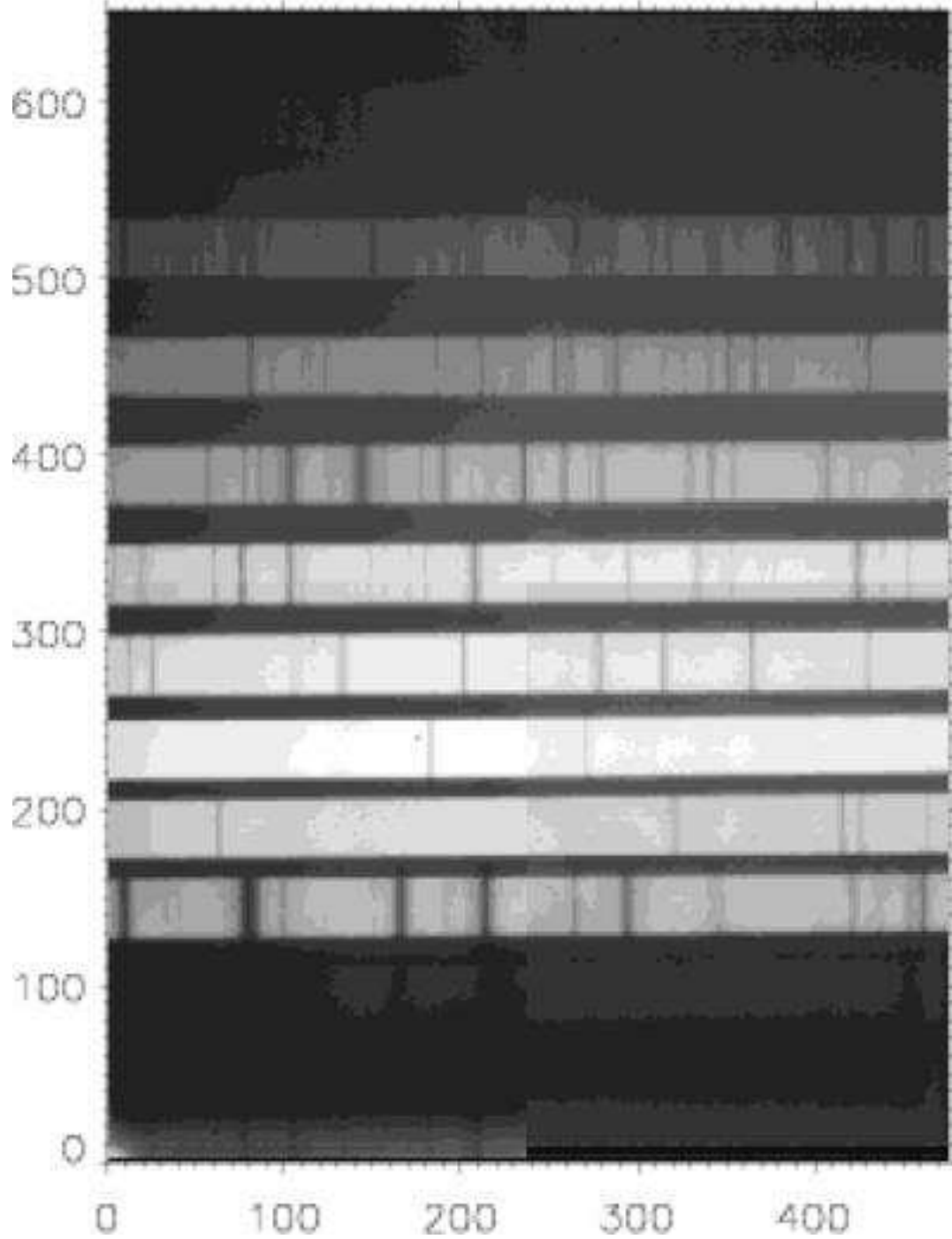


Figure 1. Cross-dispersed spectra from a telescope calibration operation. Central wavelengths in nm from top to bottom: 416, 451, 492, 541, 601, 677, 773, 902. (Note: Figure has been downsampled for Astro-ph)

Table II. DST telescope parameters retrieved with our calibration procedure. EW: Entrance window, Turr: turret mirrors, XW: Exit window. All angles are degrees.

Wavelength (nm)	400	600	800
EW retardance	2.1	-4.3	-1.2
EW orientation	12.5	12.5	12.5
Turr. rs/rp	1.12	1.08	1.11
Turr. retardance	145.1	160.1	163.4
Main rs/rp	1.00	1.00	1.00
Main retardance	179.9	179.9	179.9
XW retardance	-9.05	-3.7	-3.1
XW orientation	20.9	20.9	20.9
T-X rotation	93.3	93.3	93.3

the opposite side of the detector, which is useful for the data analysis (polarization calibration, flat-fielding and also as a reference for the thermodynamics in the inversions). Since most of the polarization signal is concentrated near the line core, it is not necessary to record both wings of the Ca lines. An additional advantage is that we can also record a strong photospheric line in the 854.2 nm images.

The old ASP modulator was used because at the time of the observations we had not yet received the new achromatic modulator from the manufacturer. This resulted in less than optimum polarimetric efficiency at these long wavelengths, especially at 1083 nm. The new modulator arrived later in the observing run and is now available for use at the DST.

4.1. MAGNETOGRAMS

Figs 2 and 3 show several maps of active region NOAA 0634 observed on June 16 at 15:16 UT. This dataset has the best seeing among our active region observations, with a granulation contrast of 3.3% (notice that this value may not be directly comparable to that of visible observations because of the variation of the source function with wavelength). Some features apparent in the magnetograms or the chromospheric filtegrams (e.g., the transversal fluctuations in the penumbral filaments near coordinates $[x = 50, y = 55]$ in the figure) exhibit spatial scales as small as $0.7''$.

The maps represented in the figures have been obtained from a spectro-polarimetric scan of the region consisting of 350 steps of $0.22''$ each.

The scanning step oversamples the resolution element. This was done so that it would be possible to bin the 10830 data in order to build up its photon count without saturating the other two detectors. Unfortunately the 1083 nm data from this day was unusable due to problems with the camera. Therefore we only show the 849.8 and 854.2 nm regions for this dataset.

The term “magnetogram” is used in this work somewhat inappropriately (but following a very widespread terminology) to refer to the amount of Stokes V signal integrated over a certain bandwidth on either the red or blue side of the line center, and normalized to the intensity integrated over the same bandwidth. We have used a 10-pixel wide square filter function. Notice that this quantity is not necessarily related to the magnetic field strength in the Sun. In some cases it may bear some resemblance to the longitudinal magnetic flux density (as defined by Graham et al. 2002), but this is not always the case (Socas-Navarro 2002) especially given the complex polarization patterns exhibited by the chromospheric lines (see Fig 4). For this reason, the red and blue magnetograms represented in Fig 2 are different. A reliable determination of the magnetic properties of the atmosphere would require the application of a realistic inversion technique, such as the one developed by Socas-Navarro et al (1998; 2000a). Such detailed study, however, is beyond the scope of the present work.

The observations reveal an intricate pattern of field/thermodynamic topologies, with remarkable differences between the photosphere and the chromosphere. The chromosphere itself looks different depending on whether we look at the red or the blue magnetograms. The blue side of the Ca II line cores is often perturbed by the occurrence of strong dynamical phenomena, resulting in very asymmetric “anomalous” polarization profiles (Socas-Navarro et al. 2000b; Socas-Navarro et al. 2000a; Socas-Navarro et al. 2001).

The red magnetograms from both Ca II lines reveal a “diffuse” pattern beyond the limb-side (right of the images) of both sunspots. Interestingly, this pattern exhibits significant differences between the two chromospheric lines. In some cases it even has the opposite polarity. For instance near the top-right corner of the images 849.8 has a mixture of black and white, whereas 854.2 is all white.

The neutral line is clearly visible on the limb-side penumbra in the photosphere (top-right panel in Fig 2), exhibiting an alternance of black and white filaments. However, the penumbral filaments in the chromosphere all have the same polarity as the umbra (black).

Notice what appear to be two network cells on the right edge (upper part of the image) of the photospheric magnetogram. The 849.8 red magnetogram shows the same structure as a chain of more isolated

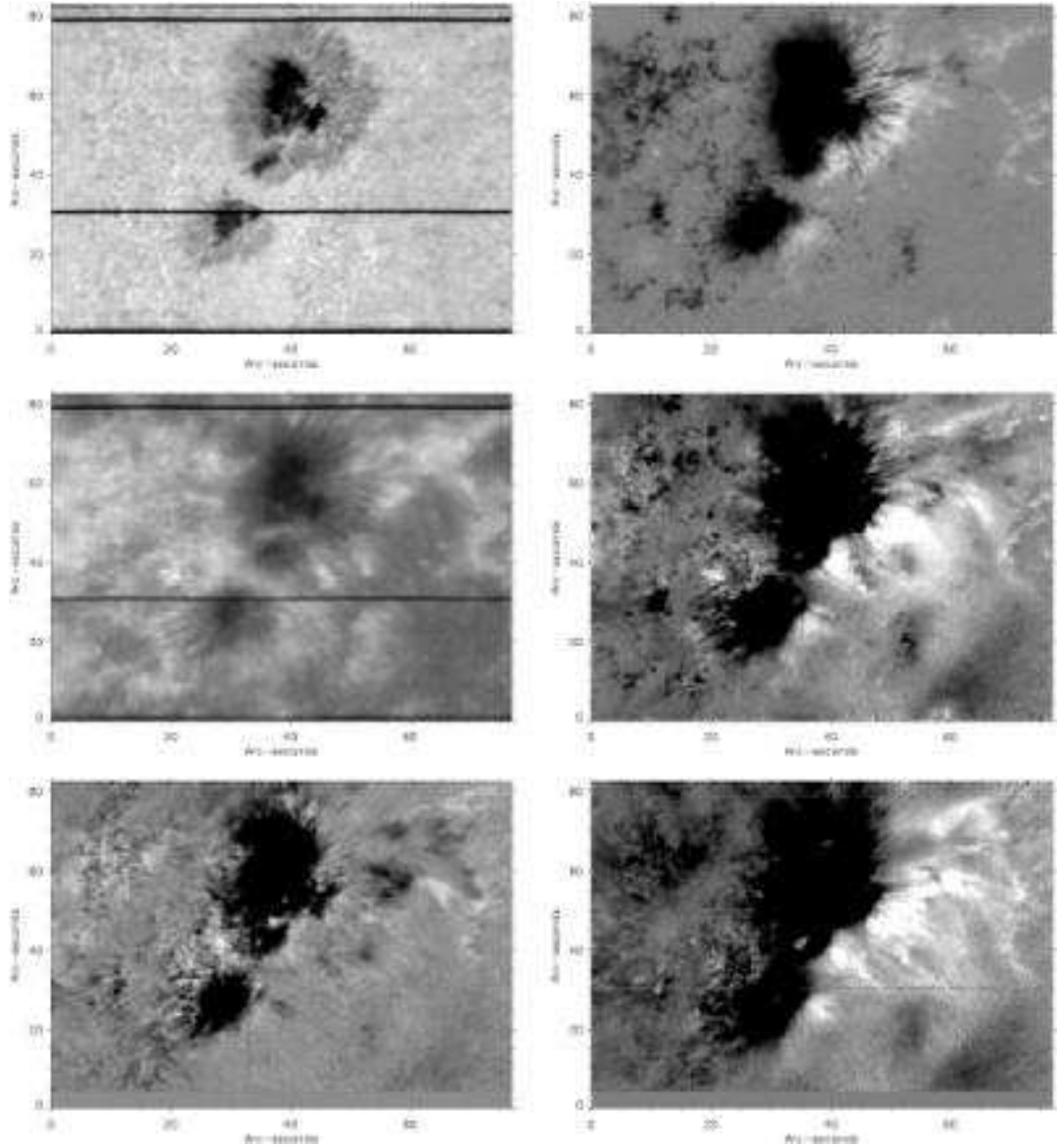


Figure 2. Various maps of active region NOAA 0634. From top to bottom, left to right: Continuum intensity. Photospheric magnetogram. Chromospheric filtergram in the core of the Ca II 854.2 nm line. Chromospheric magnetogram taken on the red side of the 849.8 nm line core. Chromospheric magnetogram on the blue side of 854.2 nm. Chromospheric magnetogram on the red side of 854.2 nm. The gray scale in all chromospheric [photospheric] magnetograms is $\pm 2\%$ [$\pm 3\%$] of the corresponding Stokes I intensity (see text). Disk center is towards the left of the image. (Note: Figure has been downsampled for Astro-ph)

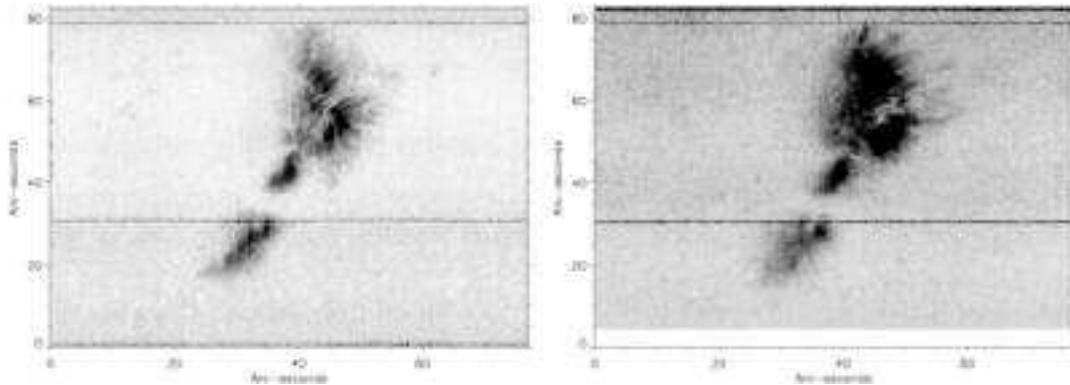


Figure 3. Magnetograms of linear polarization ($\sqrt{Q^2 + U^2}$). Left: Photospheric line (saturated at $\pm 4\%$). Right: Chromospheric Ca II line at 854.2 nm (saturated at $\pm 2\%$). (Note: Figure has been downsampled for Astro-ph)

bright knots (some of them with opposite Stokes V polarity). These cells are more difficult to discern in both (red and blue) 854.2 magnetograms. The structure of the filaments extending out of the sunspot seems to merge, at least visually, with these network cells. The upper cell interior, which is empty in the photospheric magnetogram, is filled with a diffuse field in the 849.8 magnetogram. The 854.2 image shows isolated structures in the cell interior.

A small facula that appears as a sharp black feature at coordinates $(x = 55, y = 20)$ in the photospheric magnetogram shows as a diffuse black area in 849.8 surrounded by a white region. In 854.2 the black feature is even more diffuse. At the very bottom of the photospheric image, near $x = 60$, there is a small positive (white) magnetic feature. In 849.8 this is clearly visible as two bright knots, surrounded by opposite polarity field.

The area to the left of the sunspots is also interesting. The predominantly negative polarity in the photosphere turns into a small-scale mixture of small black and white dots. The 854.2 line, however, shows again a concentration of predominantly negative polarity in the upper part.

Finally, notice how the separation between the two sunspots, which is about $5''$ in the photospheric magnetogram, becomes shorter in the 849.8 magnetogram and finally disappears when seen in 854.2.

The linear polarization signal, shown in Fig 3, is only prominent in the sunspots. The photospheric and chromospheric maps are rather similar, although the chromospheric map is more diffuse and exhibits filaments extending further away from the sunspot.

A sample of the slit spectra recorded by SPINOR is presented in Fig 4. The data in the figure are from a scan of NOAA 0635 observed on June 19 at 14:08 UT. The problems with the Pluto camera computer had been solved during the previous days, allowing us to record data at 1083 nm. The signal-to-noise ratio is quite poor due to 1) the low polarimetric efficiency discussed above, and 2) especially to the low quantum efficiency of the camera at this wavelength ($\simeq 3\%$). The 1083 nm data displayed in the figure have been binned in the scanning direction over a $1.5''$ interval. The 849.8 and 854.2 nm data are unbinned ($0.22''$).

4.2. VELOCITIES

Photospheric velocity maps of NOAA 0634 were obtained by measuring the minimum position of the Fe I line at 849.7 nm. A similar strategy is not viable for the Ca II lines, however, because of the complicated patterns of emission reversals and self-absorptions found in the line cores. Instead we measured the intensity difference between two points symmetrically located at various distances from the line core. This method is only an approximation but it seems to work better than taking the minimum position.

Fig 5 shows the velocity maps at various optical heights. The cosine of the heliocentric angle for this region is $\mu = 0.74$. Notice the two prominent dark features marked with arrows in the figure. These features are very strong plasma flows directed away from the line of sight and located on the center side of the sunspot (but further away than the photospheric penumbra). Detailed profiles of these features are shown in Fig 6.

Both features exhibit very strong redshifts, visible in Stokes I and V . Point A shows a very prominent redshift starting near 40 pm away from line center (corresponding roughly to the high photosphere or low chromosphere) all the way to the line core (middle chromosphere). This feature is well localized (see lower panel) and the Doppler shift is $\sim 14 \text{ km s}^{-1}$. Point B exhibits somewhat weaker flows ($\sim 10 \text{ km s}^{-1}$) flows that are more localized in height (upper photosphere/lower chromosphere), but has a more extended tail along the slit (see lower panel).

The polarization signal indicates that these features are of magnetic nature, perhaps the result of chromospheric plasma falling down at high speed inside a magnetic filament. Further observations with time resolution and detailed Non-LTE modeling would be desirable to understand the structure and evolution of such strong downflows.

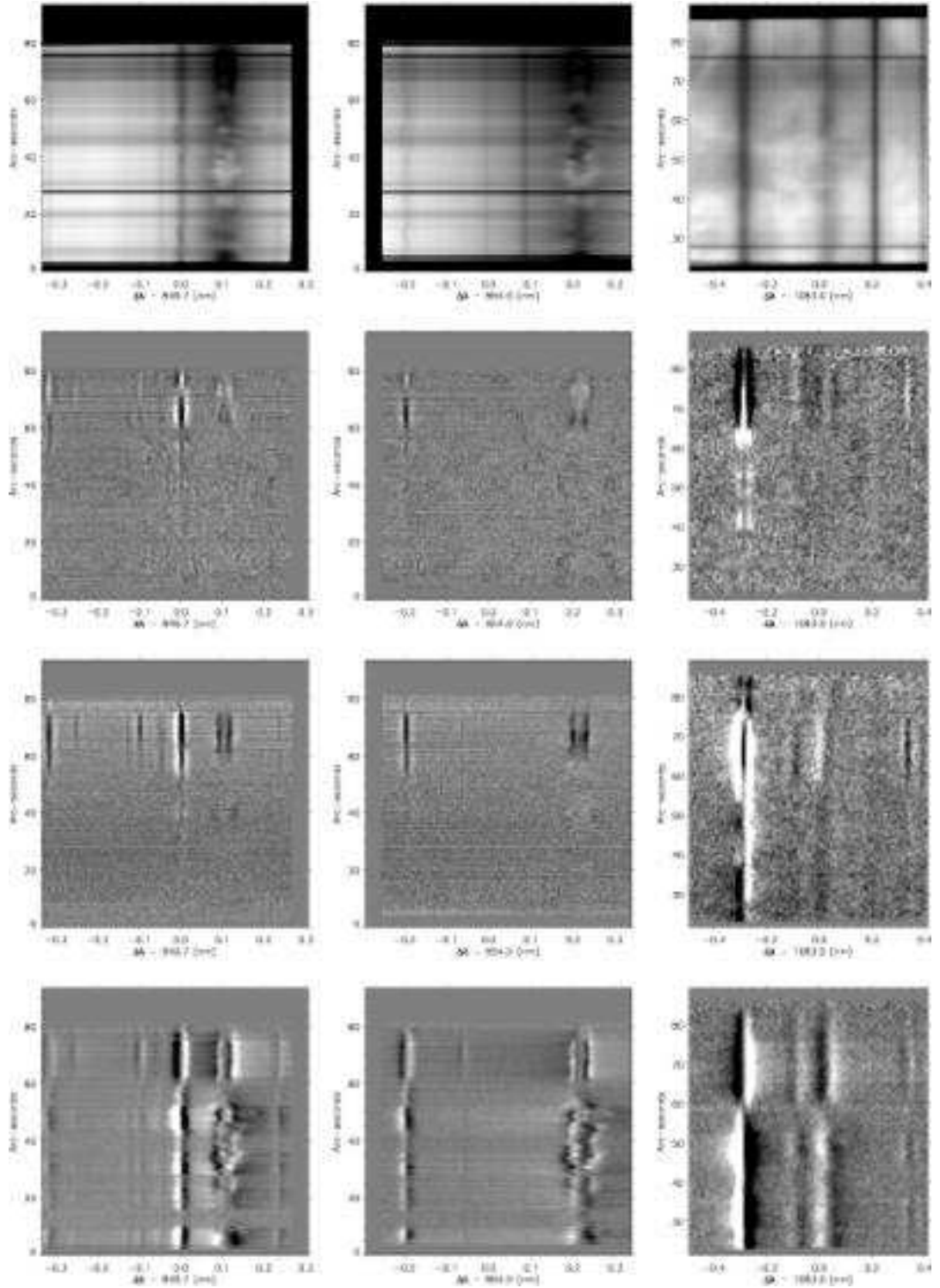


Figure 4. Stokes profiles from one particular slit position of the NOAA 0635 scan. Rows: Stokes I, Q, U and V parameters (from top to bottom). Columns: Images from the cameras at 849.8 (left), 854.2 (middle) and 1083 (right) nm. Profiles are normalized to quiet Sun continuum. Stokes Q and U panels are saturated at $\pm 1\%$, Stokes V panels are saturated at $\pm 2\%$. (Note: Figure has been downsampled for Astro-ph)

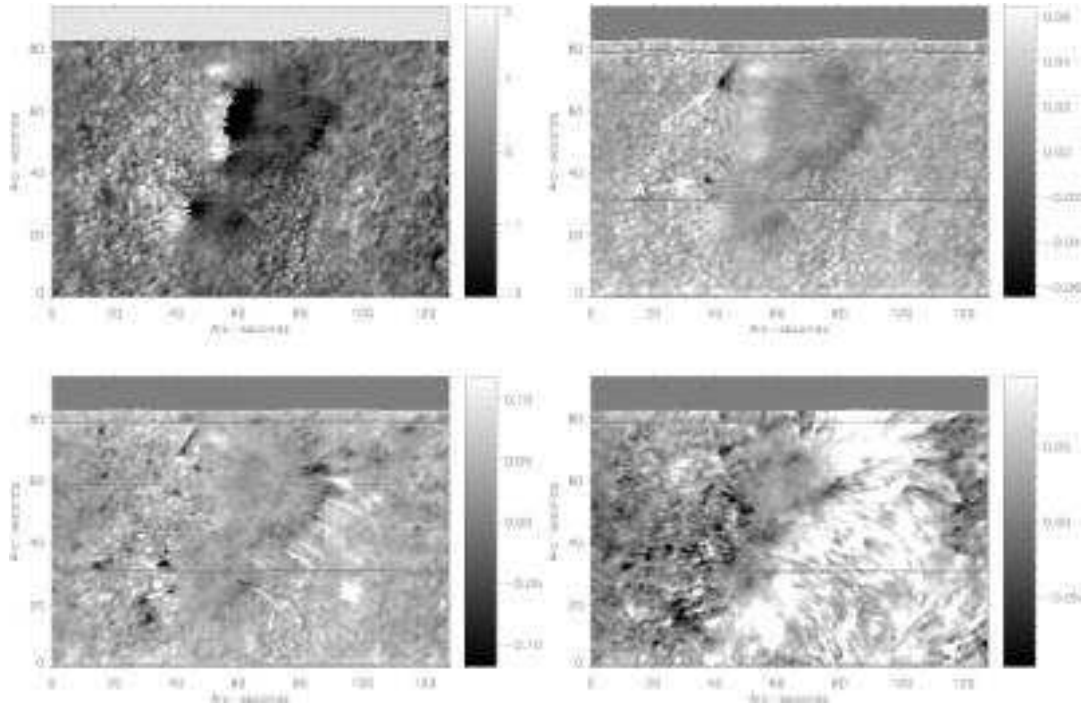


Figure 5. Upper left: Line of sight velocity measured in the core of a photospheric Fe I line (scale is km s^{-1}). Other panels: Line of sight velocity maps measured as the difference between blue and red intensity at 75, 37 and 7 pm from the 849.8 nm line center, in units of continuum intensity. In all cases (black/white) represents flows (away from/towards) the observer. The arrows mark the positions of two interesting features discussed in the text.(Note: Figure has been downsampled for Astro-ph)

5. Conclusions

This paper presents some initial results from first-light observations with SPINOR, a new facility instrument for the DST. We perceive an urgent demand in the solar community for a new experiment-oriented (as opposed to specialized) spectro-polarimeter. We expect that SPINOR will fulfill this need and remain at the cutting-edge of solar research at least until the construction of the Advanced Technology Solar Telescope (Keller et al. 2002). Its broad wavelength coverage will provide a uniquely connected view of photospheric, chromospheric and, to some extent, coronal magnetism. The observations presented in the present paper are intended to emphasize this point and to demonstrate the capabilities of the instrument in the near infrared.

It is important to remark that the final configuration of the instrument will provide significant improvements for infrared observations with respect to the performance reported here. The new achromatic

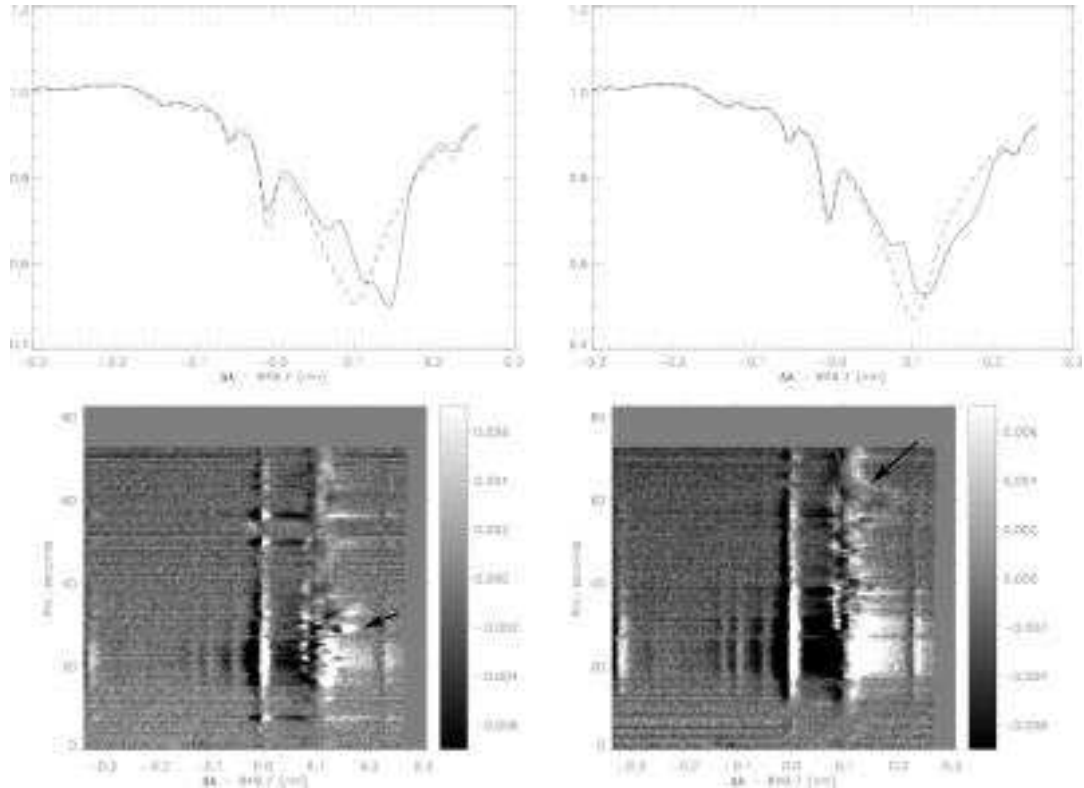


Figure 6. Upper panels: Stokes I profiles of points A (left) and B(right) normalized to quiet Sun continuum. The solid line represents the average intensity profile along the slit direction. Note the strong redshifts present in the chromospheric lines. Lower panels: Stokes V spectra at the slit positions of points A (left) and B (right) in Fig 5. The arrows mark the positions along the slit of these two points. (Note: Figure has been downsampled for Astro-ph)

modulator (already deployed) and cameras (larger format and more efficient) will hopefully enhance SPINOR's performance at $1\mu\text{m}$ and extend its range up to $1.6\mu\text{m}$.

As with the ASP, researchers from national and foreign institutions will be able to access the new instrument through the usual time allocation competition for the Dunn Telescope, operated by NSO.

6. Acknowledgments

The authors wish to acknowledge the enthusiastic support from the NSO staff at the Sac Peak observatory, especially D. Gilliam, M. Bradford and J. Elrod. Thanks are also due to S. Hegwer, S. Gregory, R. Dunbar, T. Spence, S. Fletcher, C. Berst and W. Jones.

References

- Casini, R. and A. López Ariste: 2003, ‘. In: *Solar Polarization, ASP Conference Series, held Sep 3rd-Oct 4th 2002 at Puerto de la Cruz, Tenerife, Spain. Edited by J. Trujillo Bueno and J. Sánchez Almeida. San Francisco: Astronomical Society of the Pacific, 2003. p. in press.*
- del Toro Iniesta, J. C., L. R. Bellot Rubio, and M. Collados: 2001, ‘Cold, Supersonic Evershed Downflows in a Sunspot’. *ApJL* **549**, L139–L142.
- Elmore, D. F., B. W. Lites, S. Tomczyk, A. Skumanich, R. B. Dunn, , J. A. Schuenke, K. V. Streater, T. W. Leach, C. W. Chambellan, Hull, and L. B. Lacey: 1992. In: *Proc SPIE*, Vol. 1746. p. 22.
- Graham, J. D., A. López Ariste, H. Socas-Navarro, and S. Tomczyk: 2002, ‘Inference of Solar Magnetic Field Parameters from Data with Limited Wavelength Sampling’. *Solar Physics* **208**, 211–232.
- Keller, C. U.: 1998, ‘SOLIS: a modern facility for synoptic solar observations’. *Proc. SPIE* **3352**, 732–741.
- Keller, C. U., T. R. Rimmele, F. Hill, S. L. Keil, J. M. Oschmann, and the ATST Team: 2002, ‘The Advanced Technology Solar Telescope’. *Astronomische Nachrichten* **323**, 294–298.
- Khomenko, E. V., M. Collados, S. K. Solanki, A. Lagg, and J. Trujillo Bueno: 2003, ‘Quiet-Sun inter-network magnetic fields observed in the infrared’. *A&A* **408**, 1115–1135.
- López Ariste, A., S. Tomczyk, and R. Casini: 2002, ‘Hyperfine Structure as a Diagnostic of Solar Magnetic Fields’. *ApJ* **580**, 519–527.
- Lin, H.: 1995, ‘On the Distribution of the Solar Magnetic Fields’. *ApJ* **446**, 421.
- Lin, H. and T. Rimmele: 1999, ‘The Granular Magnetic Fields of the Quiet Sun’. *ApJ* **514**, 448–455.
- Lites, B. W., D. F. Elmore, and K. V. Streater: 2001, ‘“The Solar-B Spectro-Polarimeter”’. In: M. Sigwarth (ed.): *Advanced Solar Polarimetry – Theory, Observation, and Instrumentation*, Vol. 236 of *ASP Conf. Ser.* p. 33.
- Manso Sainz, R. and J. Trujillo Bueno: 2001, ‘Modeling the Scattering Line Polarization of the Ca II Infrared Triplet’. In: *ASP Conf. Ser. 236: Advanced Solar Polarimetry – Theory, Observation, and Instrumentation.* p. 213.
- Martínez Pillet, V., B. W. Lites, A. Skumanich, and D. Degenhardt: 1994, ‘Evidence for supersonic downflows in the photosphere of a delta sunspot’. *ApJL* **425**, L113–L115.
- Martínez Pillet, V.: 2000, ‘Spectral signature of uncombed penumbral magnetic fields’. *A&A* **361**, 734–742.
- Martínez Pillet, V.: 2001, ‘Spectral signature of uncombed penumbral magnetic fields. Reply’. *A&A* **369**, 644–645.
- Rimmele, T. R.: 2000, ‘Solar adaptive optics’. In: *Proc. SPIE Vol. 4007, p. 218-231, Adaptive Optical Systems Technology, Peter L. Wizinowich; Ed.* pp. 218–231.
- Sánchez Almeida, J.: 2001, ‘Spectral signature of uncombed penumbral magnetic fields. Comment’. *A&A* **369**, 643.
- Sánchez Almeida, J. and J. A. Bonet: 1998, ‘The Spectrum of Fluctuations across Penumbral Filaments’. *ApJ* **505**, 1010–1017.
- Sankarasubramanian, K., D. F. Elmore, B. W. Lites, M. Sigwarth, T. R. Rimmele, S. L. Hegwer, S. Gregory, K. V. Streater, L. M. Wilkins, K. Richards, and C. Berst: 2003, ‘Diffraction limited spectro-polarimeter - Phase I’. In: *Polarimetry in Astronomy. Edited by Silvano Fineschi . Proceedings of the SPIE, Volume 4843, pp. 414-424 (2003).* pp. 414–424.

- Schlichenmaier, R.: 2002, ‘Penumbral fine structure: Theoretical understanding’. *Astronomische Nachrichten* **323**, 303–308.
- Schmidt, W., C. Beck, T. Kentischer, D. Elmore, and B. Lites: 2003, ‘POLIS: A spectropolarimeter for the VTT and for GREGOR’. *Astronomische Nachrichten* **324**, 300–301.
- Skumanich, A., B. W. Lites, V. Martínez Pillet, and P. Seagraves: 1997, ‘The Calibration of the Advanced Stokes Polarimeter’. *ApJS* **110**, 357.
- Socas-Navarro, H.: 2002, ‘Zeeman diagnostics of solar magnetic fields’. In: *SOLMAG 2002. Proceedings of the Magnetic Coupling of the Solar Atmosphere Euroconference and IAU Colloquium 188, 11 - 15 June 2002, Santorini, Greece*. Ed. H. Sawaya-Lacoste. ESA SP-505. Noordwijk, Netherlands: ESA Publications Division, ISBN 92-9092-815-8, 2002, p. 45 - 51. p. 45.
- Socas-Navarro, H.: 2003, ‘Small-scale Magnetic Fields in the Quiet Sun’. In: *Solar Polarization, ASP Conference Series, held Sep 3rd-Oct 4th 2002 at Puerto de la Cruz, Tenerife, Spain*. Edited by J. Trujillo Bueno and J. Sánchez Almeida. San Francisco: Astronomical Society of the Pacific, Vol 307. p. 330.
- Socas-Navarro, H., B. Ruiz Cobo, and J. Trujillo Bueno: 1998, ‘Non-LTE Inversion of Line Profiles’. *ApJ* **507**, 470–481.
- Socas-Navarro, H. and J. Sánchez Almeida: 2002, ‘Magnetic Properties of Photospheric Regions with Very Low Magnetic Flux’. *ApJ* **565**, 1323–1334.
- Socas-Navarro, H. and J. Sánchez Almeida: 2003, ‘Magnetic Fields in the Quiet Sun: Observational Discrepancies and Unresolved Structure’. *ApJ* **593**, 581.
- Socas-Navarro, H., J. Trujillo Bueno, and B. Ruiz Cobo: 2000a, ‘Anomalous Circular Polarization Profiles in Sunspot Chromospheres’. *ApJ* **544**, 1141–1154.
- Socas-Navarro, H., J. Trujillo Bueno, and B. Ruiz Cobo: 2000b, ‘Anomalous Polarization Profiles in Sunspots: Possible Origin of Umbral Flashes’. *Science* **288**, 1396–1398.
- Socas-Navarro, H., J. Trujillo Bueno, and B. Ruiz Cobo: 2000c, ‘Non-LTE Inversion of Stokes Profiles Induced by the Zeeman Effect’. *ApJ* **530**, 977–993.
- Socas-Navarro, H., J. Trujillo Bueno, and B. Ruiz Cobo: 2001, ‘A Time-dependent Semiempirical Model of the Chromospheric Umbral Oscillation’. *ApJ* **550**, 1102–1112.
- Solanki, S. K., W. Curdt, A. Gandorfer, M. Schüssler, B. W. Lites, V. Martínez Pillet, W. Schmidt, A. M. Title, and The Sunrise Team: 2003, ‘SUNRISE: Balloon-borne High-Resolution Observation of the Sun’. *Astronomische Nachrichten Supplement* **324**, 113–+.
- Uitenbroek, H.: 1989, ‘Operator perturbation method for multi-level line transfer with partial redistribution’. *A&A* **213**, 360–370.

